ACS APPLIED MATERIALS & INTERFACES
Research Article
www.acsami.org

Easy Route to the Wettability Cycling of Copper Surface between Superhydrophobicity and Superhydrophilicity

Guoyong Wang and Tong-Yi Zhang*

Department of Mechanical Engineering, Hong Kong University of Science and Technology, Clearwater Bay, Kowloon, Hong Kong SAR, P. R. China

Supporting Information

ABSTRACT: A hierarchical copper structure combining micro- and nano-gaps/pores was built up on copper substrate by etching and electrodeposition. The fresh as-deposited copper was easily oxidized in air at room temperature, forming a CuO layer covering on the surface. The surface could be hydrophobized with thiol-modified fluorocarbons, after which it showed a water contact angle as high as 165° ± 2°. This surface could also regain the superhydrophilicity with a zero water contact angel after annealing at 200 °C for 10 min to desorb the low surface energy monolayer of thiol-modified fluorocarbons and reform a CuO layer again on the surface. Repeating the process of adsorption/desorption of the monolayer by modification and annealing, it was successful to fulfill the wettability cycling between superhydrophobicity and superhydrophilicity on the copper surface. The adsorption and desorption mechanism of the monolayer was discussed based on the result of surface chemistry analysis.

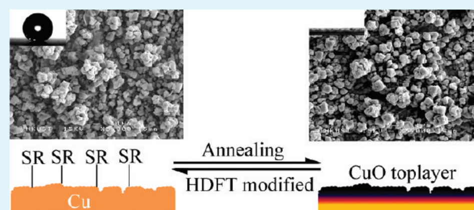

KEYWORDS: *materials science, surface chemistry, CuO, wettability cycling, desorption*

INTRODUCTION

Superhydrophobic surfaces have attracted great interest because of their potential applications in various areas, such as self-cleaning, antisticky, anticorrosion, drag-reduction coating, drug delivery, microfluidic devices, intelligent membranes, and in lab-on-chip systems.[1−17] Synthetic superhydrophobic surfaces are generally obtained by combining micro/nanostructures with low surface energy, on which air pickets are trapped below the water droplet, as shown in a typical Cassie case, resulting in large contact angles (>150°) and low sliding angles(<10°). Solid surfaces with switchable wettability between superhydrophobicity and superhydrophilicity are of great importance due to their numerous industrial applications.[18] Usually, the switchable wettability is achieved by changing the surface chemistry rather than surface morphology, which is implemented in experiments by external stimuli and exchange of counterions.[19,20] This is because appropriate surface morphology plays a crucial role in either superhydrophilic or superhydrophobic surface, which makes a hydrophilic surface more hydrophilic and a hydrophobic surface more hydrophobic,[21,22] as predicted by Wenzel's law and Cassie-Boxter's law.[23] As a typical example, the reversibly switchable wettability between superhydrophobicity and superhydrophilicity of the V_2O_5 film with roselike surface morphology was realized by switching on and off UV light,[24] whereas during the process, the roselike morphology was basically maintained unchanged. Other inorganic semiconductor oxides, such as TiO_2, ZnO, SnO_2, WO_3, and Ga_2O_3, possess the same switching capability as V_2O_5 as long as an appropriate surface morphology is obtained.[15,18,25,26] Organic materials containing photochromic functional groups, such as azobenzenes,[19] have the ability to undergo reversible transition of conformation triggered by UV/visible irradiation, leading to changes in their wetting properties.[27]

Most of metals and metal oxides have high surface energy, and consequently their flat surfaces have low contact angles.[28−30] When these surfaces are roughed to have appropriate surface morphology[24] and then modified with a low surface energy self-assembled monolayer,[31] the surfaces will have much high contact angles and become superhydrophobic. If one can find an easy way to adsorb/desorb the low-surface-energy monolayer without damaging the appropriate surface morphology, one will be able to cycle the surface wettability between superhydrophobicity and superhydrophilicity. Because a low energy thiol-modified fluorocarbon monolayer can be easily self-assembled on metal/metal oxide surfaces by just immersing the sample into thiol-modified fluorocarbon solution for a while, the key issue is how to desorb the layer and meanwhile keeping the surface morphology. Gu et al.[32] proposed to use HNO_3 as the monolayer eliminator and meanwhile use an Ag layer to protect the surface morphology of the substrate.

Copper-based surfaces are rather easily rendered superhydrophobic. Many research work has been conducted on the superhydrophobic behaviors of Cu-based surfaces including Cu microcabbages with CuO surfaces[33] and Cu nanowires with $Cu(OH)_2$ surfaces[34] and Cu foams[35] and patterns,[36,37] and copper tubes.[38] However, the wettability cycling of Cu-based surfaces between superhydrophobicity and superhydrophilicity

Received: September 27, 2011
Accepted: December 7, 2011
Published: December 8, 2011

 © 2011 American Chemical Society

has been seldom investigated. In this present work, we develop a convenient strategy to achieve the wettability cycling on copper surfaces though adsorbing/desorbing a low surface energy monolayer, which will not damage the basic feature of surface morphology. The appropriate surface morphology was built-up by chemical etching and electrodepostion. After the roughed sample was immersed in a 1H,1H,2H,2H-perfluorodecanethiol (HDFT) ethanol solution for 30 min, the sample had high contact angel of 165° ± 2°. The low surface energy monolayer was easily desorbed by annealing at 200 °C in air for 10 min, which turned the surface back to superhydrophilic with zero contact angle.

EXPERIMENTAL SECTION

Polycrystalline copper plates (99.99%, Goodfellow Ltd.) with thickness of 0.25 mm were selected as the substrate material. The plates of 2 cm × 2 cm were etched at room temperature in solution of 25 g $CuCl_2$ (BDH Ltd.), 25 mL HCl (37%, Sigma-Aldrich Ltd.), and 75 mL of deionized water for 30 min, followed by ultrasonification in 1 M HCl aqueous solution for 10 min to remove any residual $CuCl_2$.[31] After that, the samples were rinsed with deionized water rapidly, and then dried with compressed air. Then, Cu electrodeposition was carried out on these etched surfaces at a constant potential of 1.5 V at room temperature in stationary electrolyte without stirring or air bubbling, where the electrolyte was an aqueous solution containing $CuSO_4$ (0.5 M, Scharlau Ltd.) and H_2SO_4 (1.5 M, Acros Ltd.). The working electrode, kept 2 cm away from the anode, was a clean and polished copper plate with the same size as the cathode. Electrodeposition time varied from 7 to 30 s and after the deposition, the samples were rinsed with deionized water, dried with compressed air and then kept in a desiccator for further experiments.

To absorb a surface layer with low surface energy, the samples were immersed in 1 mM HDFT-ethanol solution for 30 min, followed by washing in ethanol and then drying with compressed air. The low-energy surface layer was desorbed by annealing the samples at a temperature 200 °C in air for 10 min.

The morphology of the as-electrodeposited, modified and annealed copper surfaces were examined using a scanning electron microscope (JEOL 6300F). The average surface roughness (Ra) was determined by an optical profiler (Wyko NT3300, Vecco) in the vertical scanning interferometry (VSI) mode with 1 nm resolution. The scanning area was 231.7 μm × 304.4 μm. Five locations on a sample were scanned and their average roughness was reported here. The microstructure of the deposited copper clusters was characterized using a transmission electron microscope (TEM, JEOL 2010F). To prepare the TEM samples, the copper deposits were scraped away from the substrate by a blade and then the copper power was suspended into ethanol, which was then dropped on a carbon-coated Cu grid for the TEM observations. The static contact angel (CA) measurements were completed on a Digidrop (GBX, France). Distilled water droplets with each having a volume of 4 μL were used in the contact angle tests. X-ray photoelectron spectroscopic (XPS) tests were conducted with a surface analyzer (Kratos Axis Ultra DLD) using an Al Kα source working at 14 kV and 25 mA. Peak areas were calculated after the background subtraction by using the hybrid Shirley and linear method.

RESULTS AND DISCUSSION

Images a and b in Figure 1 show the surface morphology after etching in $CuCl_2$ solution for 30 min. The chemical reaction was more significant along grain boundaries, resulting in the morphology that valleys were formed along the grain boundaries. Some grains exposed on the surface were etched out, and the others pop out for ridges forming inside the grains. The etching enhances the surface roughness from Ra = 129.41 nm to Ra = 309.55 nm, as measured from the optical profiler images a and b in Figure 2. The etched rough surface and the use of acidic electrolyte, which generates hydrogen gas and will be discussed later, lead to the island growth mode in the following Cu electrodeposition. Figure 1c−j)are SEM images, showing the morphology evolution of the copper surface. When the deposition time is about 7 s, the substrate is sparsely covered by deposited Cu crystals of the diameters mainly in the range of 100 to 400 nm, as shown in Figure 1c, d. Some clusters with the diameters in the range of 1 to 2 μm were formed on the ridges. As the deposition going on, the coverage area of the substrate surface increased and the size of deposited Cu clusters also increased. Images e and f in Figure 1 show the surface morphology at the deposition time of about 15 s, indicating that the diameter of some clusters increases to round 3 μm. Meanwhile, many copper crystals were electrodeposited at the valleys. The coverage of deposited Cu on the substrate increased obviously with deposition time, which is shown clearly by comparing the surface morphology, Figure 1g, h, at deposition time of 23 s to that, Figure 1e, f, at deposition time of 15 s. Images i and j in Figure 1 confirm that the surface was completely covered by the deposited copper after 30 s deposition. During the deposition, the electrochemical reactions taking place at the cathode surface (copper plate) include copper-ion reduction and hydrogen gas formation. Hydrogen gas is a byproduct of the deposition in such acidic electrolyte, and using a

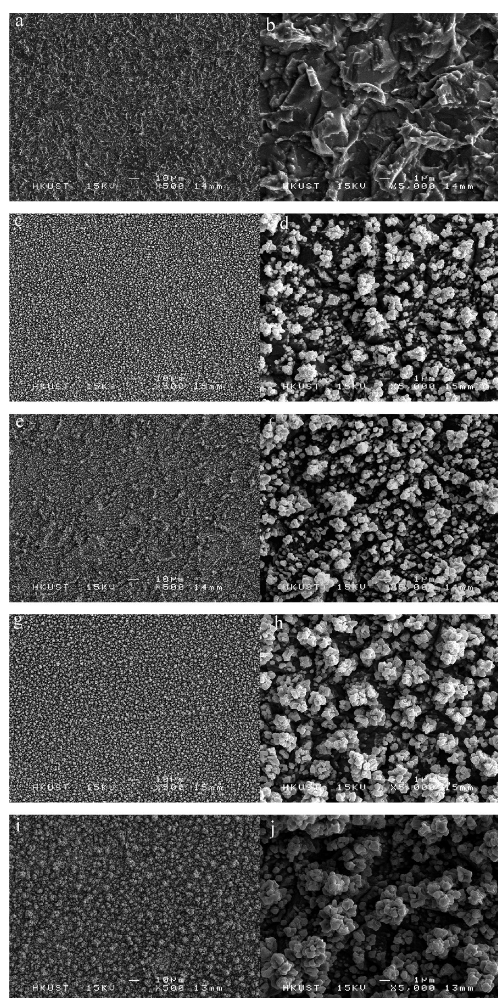

Figure 1. Topographical evolution of copper crystals deposited on copper plates with increasing time (a, b) 0, (c, d) 7, (e, f) 15, (g, h) 22, and (i, j) 30 s. b, d, f, and h are the enlarged images of a, c, e, g, and i, respectively.

dx.doi.org/10.1021/am2013129 | ACS Appl. Mater. Interfaces 2012, 4, 273−279

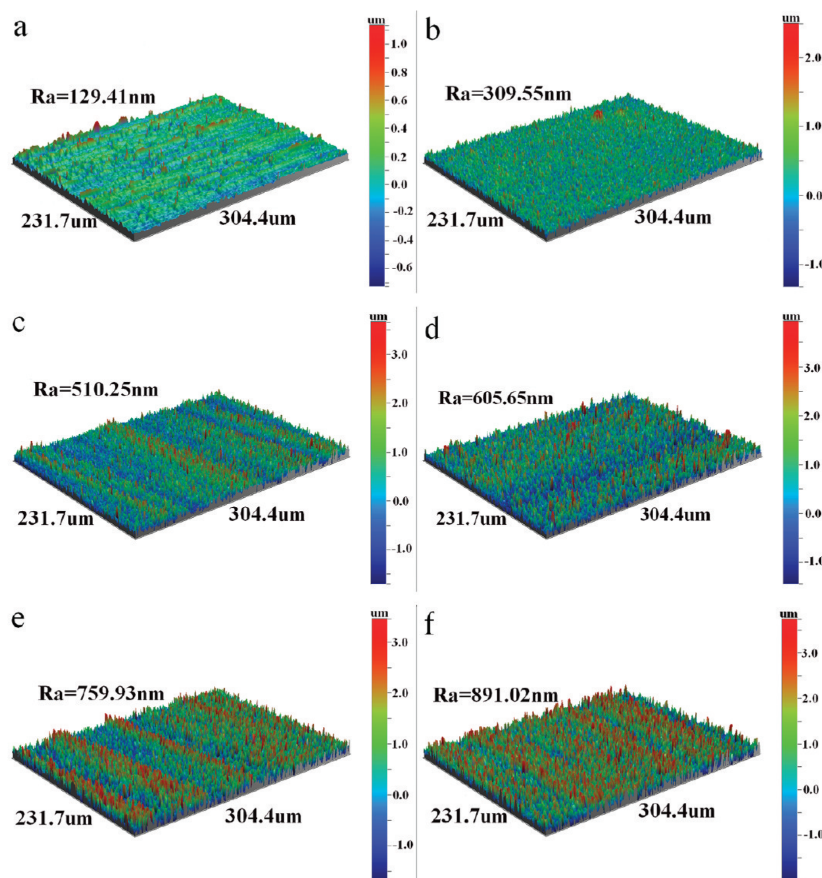

Figure 2. (a) Surface roughness of naked copper plate and (b) its evolution after etching and followed by electrodepostion with increasing time (c) 7, (d) 15, (e) 22, and (f) 30 s.

relatively low overpotential forms more quasi-static hydrogen bubbles, which provide simultaneously constraint to the reduction of copper ions. Electrolyte and copper ions are repelled by the bubbles, and copper crystals are guided to deposit and grow only at the interstices of these bubbles. Moreover, a partial current is directed to the formation of hydrogen gas at the freshly deposited copper surface. The small amount of hydrogen that is slowly formed leads to the separation of the copper crystals and formation the nanogaps/pores between them. The etched cathode surface is rough and electrodeposition always concentrates at summits of the rough surface, which results in that more copper atoms are deposited at the summits and grown to copper crystal clusters there. Due to this electrodeposition mechanism, the surface roughness increases with the deposition time. The roughness increases from Ra = 510.25 nm to Ra = 891.02 nm, when the deposition time increases form 7 to 30 s, as shown in Figure 2. The distance between copper clusters is about 2−3 μm after 30 s electrodeposition, as shown in images i and j in Figure 1.

Figure 3a is a TEM image of the deposited Cu cluster, whereas the inset is the corresponding selected area diffraction (SAD) pattern of the area marked with the white rectangle. The marked rectangle area is about 300 nm ×400 nm, but it still contains several crystals with diameters at several tens of nanometers, as conformed by the SAD pattern. The diffraction pattern of CuO is also identified, as indicated by the white arrows in the inset. This is because that fresh as-deposited copper surface is easy to react with oxygen in air at room

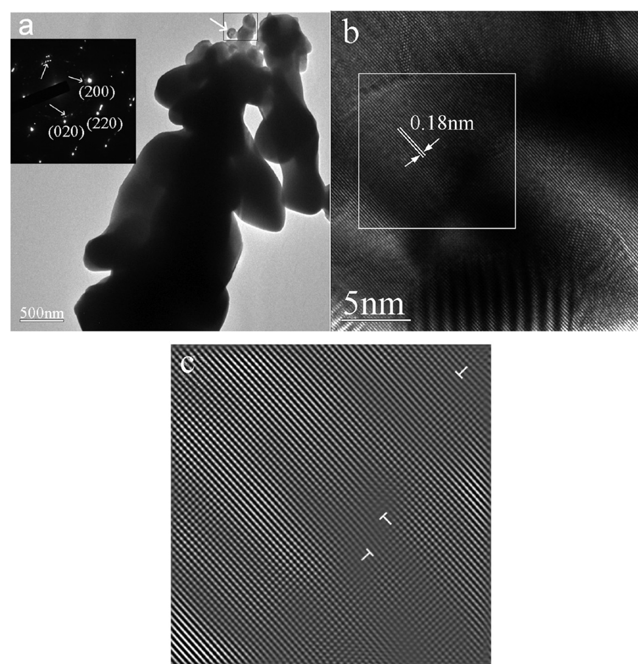

Figure 3. (a) TEM image of a cluster of copper crystals, the inset is the electron diffraction pattern of the area marked by the white square. (b) HRTEM of the region marked by the arrow in a. (c) Image of inverse fast Fourier transformation of the region marked by the square in b.

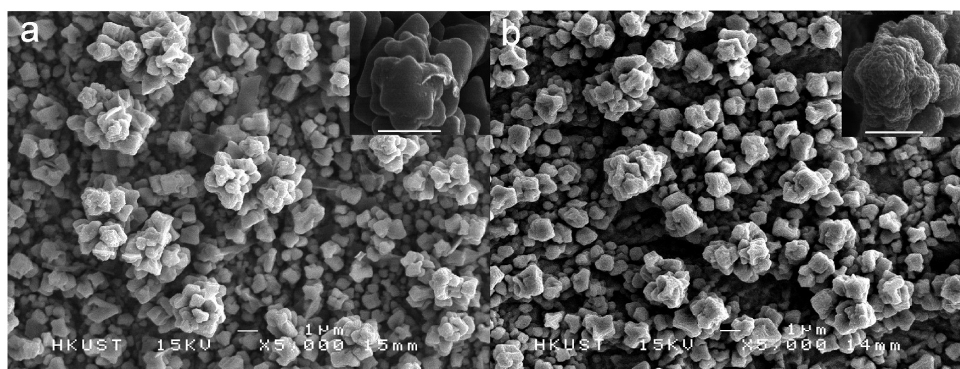

Figure 4. SEM Images of the surface morphologies: (a) after electrodepostion for 30 s and modification by HTDF for 30 min and (b) after annealed at 200 °C for 10 min. A high resolution SEM image of a representative cluster is shown in each inset, respectively, where the scale bar represents 1 μm.

temperature and that is why CuO is often observed on the fresh deposited Cu.[39] Figure 3b is a high-resolution TEM image of the edge part marked by the white arrow in Figure 3a, showing a lattice fringe of 0.18 nm corresponding to the Cu (200) lattice spacing. Besides, Moire fringes appear in Figure 3b, at the bottom of this image, which is caused by overlapping of underneath Cu crystal particle with a diameter of about 10 nm. Figure 3c is an inverse fast Fourier transform pattern (FFT) of the area marked by a white square in Figure 3b, exhibiting three edge dislocations, which indicates that even such nanocrystals still contain defects like dislocations.

After the surface modification by immersing it in the 1 mM HDFT-ethanol solution for 30 min, the surface remains its original morphology, as shown by comparing the SEM image in Figure 4a with that in Figure 1j. The modified surface is superhydrophobic with water contacted angle of 165° ± 2°. Figure 5a shows a photo of a water droplet on the superhydrophobic surface. If titling the sample gently, the droplet lunged forward and finally slid downward as the tilted angle was less than 1°. The contact angle was measured again on the same modified surface after the sample was kept in air at room temperature for a month. The one-month-aged sample exhibits the same superhydrophobic behavior, indicating that the superhydrophobic surface is reliable in air at room temperature. However, if we annealed the sample at 200 °C for 10 min, we changed the surface to be superhydrophilic. After annealing, the CA measurement gave a zero contact angle because the water droplet was absorbed quickly once it was on the surface. Figure 5b shows that the upper side of the substrate is bright because the gaps/pores there are filled with water. Figure 4b is a SEM image of the annealed surface. Comparing Figure 4b to Figure 4a indicates that the surface morphology after annealing is almost the same as that after modification. However, high-resolution SEM images, the insets in a and b in Figure 4, indicate that after the desorption of the monolayer with low surface energy, there are nanoscaled wrinkles on the cluster surface, implying that the monolayer coating smoothens the wrinkles at the nanometer scale. When the annealed sample was immersed in the 1 mM HDFT-ethanol solution for 30 min, the surface recovered its superhydrophobicity with the same contact angle of 165° ± 2°. The wettability change was cycled ten times. Figure 5c shows the experimental result, indicating the excellent reversibility of the surface wettability. The excellent reversibility will continue until the appropriate surface roughness is damaged. The wettability cycling, in some sense, likes fatigue, meaning that accumulated damage might occur during the cycling. When the cycling number is small, damage is not detectable for a given characterization facility, whereas damage becomes detectable when the cycling number exceeds a critical value, which depends on the sample property and the cycling treatment. It is extremely important in the application of wettability cycling (or switching) between superhydrophobicity and superhydrophilicity. However, no report can be found in the literature about the wettability cycling (or switching) fatigue. After ten times of wettability cycling, no detectable change or damage was observed in the CuO surface, indicating that the wettability cycling (or switching) fatigue test might take much longer time, which will be the task of our future research. Each cycle of the wettability change of the Cu surfaces takes less than 40 min in the newly developed route, which is longer than 25 min of the WO_3 surfaces.[32] However, if the wettability cycling is induced by UV illumination, each cycle takes several days.[9] It is obvious that the faster the wettability cycling is, the wider its applications will be. How to enhance the wettability cycling speed is still a great challenge to academics and industry.

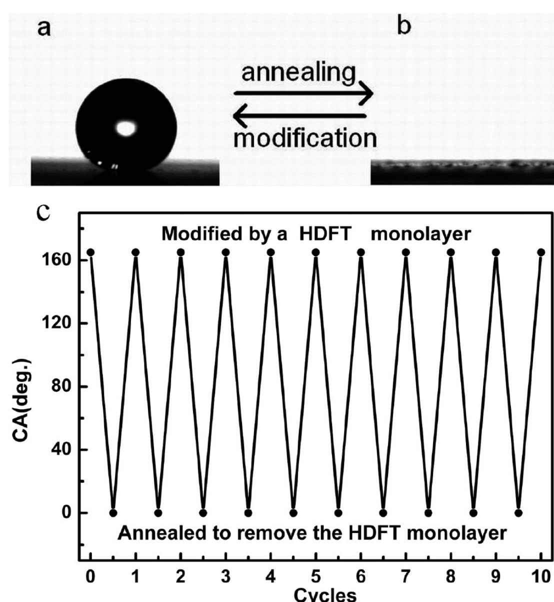

Figure 5. Photographs of (a) a water droplet on the modified surface and (b) a water droplet on the annealed surface; (c) cycles between superhydrophobicity and superhydrophilicity for the prepared surface under modification for 30 min and annealing at 200 °C for 10 min.

Figure 6a shows the X-ray photoelectron (XP) spectra of the electrodeposited copper surface before the surface modification, which is called the naked sample, and after the surface modification. The XP spectrum from the naked sample reveals the Cu(LMM) peak at 569.6 eV, Cu(2p) peak at 932.8 eV, O(1s) peak at 531.2 eV, C(1s) peak at 284.8 eV. After the

dx.doi.org/10.1021/am2013129 | ACS Appl. Mater. Interfaces 2012, 4, 273−279

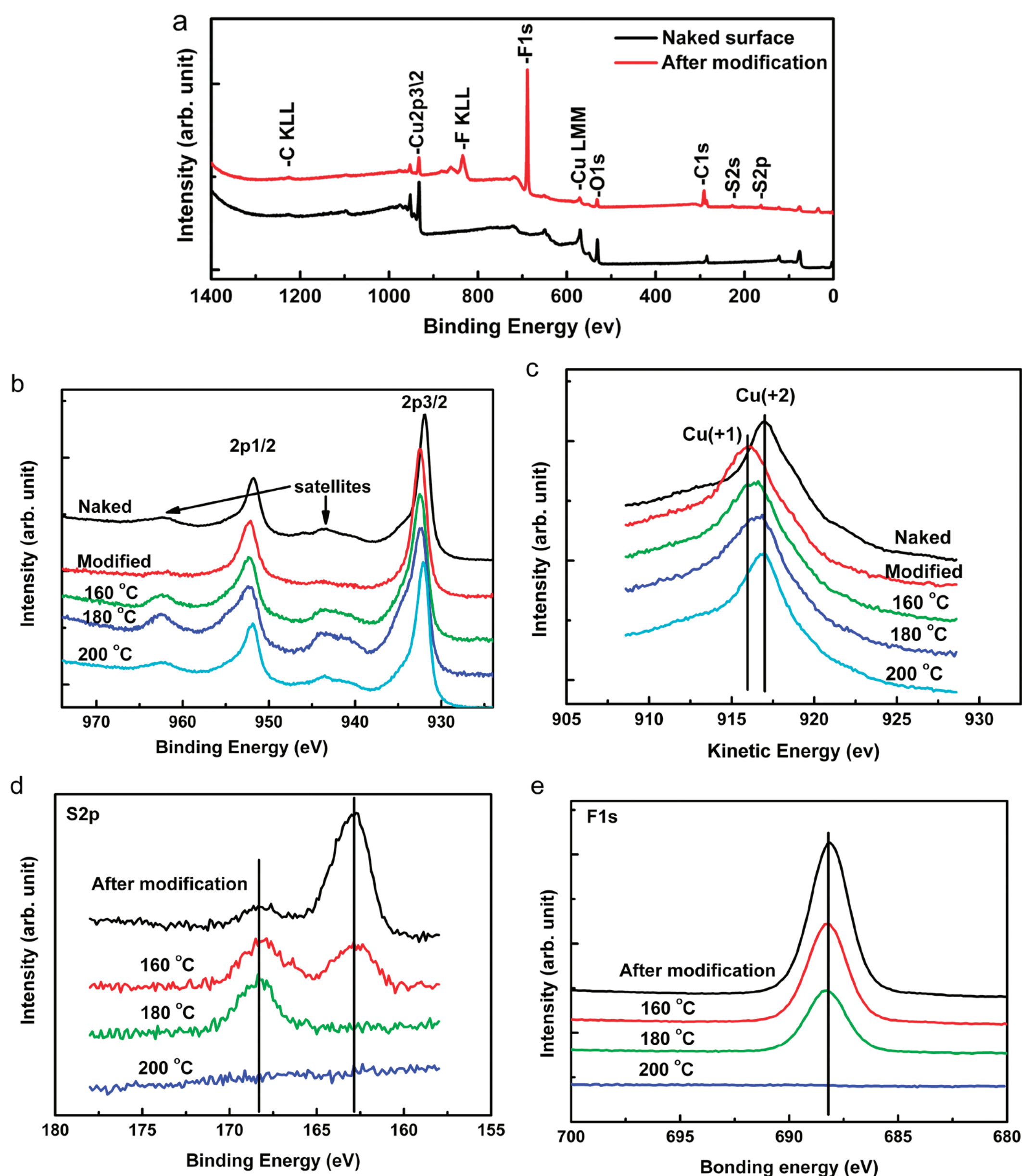

Figure 6. (a) XP survey spectra of electrodeposited copper surface before and after modification. XP high-resolution spectra revolution of (b) Cu(2p) regions, (d) S(2p) regions, (e) F(1s) regions, and (c) Auger spectra of the Cu(LMM) regions as function of annealing temperature.

surface modification, as expected, the XP spectrum exhibits more peaks including F(1s) peak at 688.8 eV, F(KLL) peak at 834.4 eV, S(2s) peak at 227.2 eV, and S(2p) peak at 163.2 eV, than those in the XP spectrum detected from the naked sample. The XPS results confirm the presence of an HDFT monolayer on the surface after the surface modification. This monolayer terminated by nonpolar groups of $-CF_3$ possesses low surface energy, which leads to the superhydrophobicity.[19]

Figure 6b shows high-resolution XP spectra covering only the Cu(2p) peak region before and after the surface modification. The most important character in high resolution XP spectrum is the shakeup satellites, which are induced by the interaction between photoelectrons and valence electrons. The satellites are indicators of the presence of CuO.[40] The satellites are observed on the naked sample, indicating that CuO was formed on as-deposited fresh copper surface in air, which is consistent with the SAD pattern result. But the satellites disappear after the surface modification, which may imply that the Cu (2+) ions on the surface are reduced. Figure 6b also shows the copper chemical state evolution after annealing at temperatures of 160 °C, 180 °C, and 200 °C. The satellites of the Cu (2p) peaks show up again after annealing at 160 °C, which indicates that CuO is formed again after 160 °C annealing. A CuO layer could also form at higher annealing temperatures of 180 and 200 °C, as the XP high-resolution spectra of Cu (2p) regions contain obvious satellites of the main core-level peaks. Because the Cu (1+) and Cu (0) have almost the same XP spectra in the Cu (2p) region, the Auger surface analysis was conducted in the Cu(LMM) region to clarify this issue and the Auger spectra are shown in Figure 6c. The Auger spectra indicate that the Cu (LMM) peak shifts from 916.98 eV(which is assigned to Cu^{2+}) in the naked sample to 915.98 eV (which is assigned to Cu^{1+}) in the sample after the surface modification. The result shows that after the surface modification, Cu^{2+} ions are reduce to Cu^{1+}. The HDFT monolayer is not physically contact on the CuO surface, but chemically bonded to Cu by the following

reactions.[40−42] The first step is to reduce CuO to Cu_2O. Once Cu_2O is formed, RSH will react with it to form the HDFT monolayer. The chemical reactions are expressed by

$$2RSH + 2CuO \rightarrow (RS)_2 + Cu_2O + H_2O \quad (1)$$

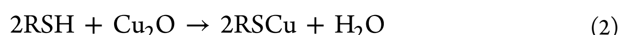

$$2RSH + Cu_2O \rightarrow 2RSCu + H_2O \quad (2)$$

As analyzed above, the monolayer is directly bonded with Cu atoms by forming a compound. The strong chemical bond determines that this monolayer cannot be washed away by organic solution, such as ethanol or acetone. It needs more energy to break the chemical bond for the wettability change. Annealing provides such high thermal energy. Figure 6c shows that after annealing at 160 °C, the peak is between the Cu (1+) and Cu (2+) peaks. We believe that the peak between the Cu (1+) and Cu (2+) peaks is a mixed peak of Cu (1+) and Cu (2+) and its position depends on the ratio of Cu (1+) and Cu (2+) contributions. The more the Cu (2+) contribution is, the closer the mixed peak to the Cu (2+) peak will be. As expected, the mixed peak is closer to the Cu (2+) peak after 180 °C annealing and completely comes back to the original Cu (2+) position after 200 °C annealing. The Auger spectra imply that the outmost surface is a CuO layer again after annealing at 200 °C and the CuO layer makes the surface superhydrophilicity.

Panels d and e in Figure 6 show high-resolution XP spectra in the S(2p) and F(1s) regions, respectively, for the modified surface annealing at temperatures of 160, 180, and 200 °C. The S(2p) peak at 162.8 eV and F(1s) peak at 688.1 eV from the sample just after the surface modification are the highest in comparing to the corresponding peaks after annealing, indicating the presence of the HDFT monolayer on the surface. If the annealing temperature is lower than 160 °C, the change in intensity of the S(2p) and F(1s) peaks is relatively small. After annealing at 160 °C for 30 min, the intensities of the S(2p) and F(1s) peaks decrease, while the peak at 168.3 eV increases. The S(2p) peak at 162.8 eV is assigned to thiolate and the peak at 168.3 eV is assigned to sulfonate.[40] When the annealing temperature is 180 °C, the S(2p) peak at 162.8 eV disappears, leaving the peak at 168.3 eV lonely. If the annealing temperature raises to 200 °C, the S(2p) and F(1s) peaks disappear completely. These observations suggest that the HDFT monolayer on the CuO surface is removed through the oxidation of the thiolate group.

On the basis of the developed route to the wettability cycling of copper surface between superhydrophobicity and superhydrophilicity, we may find wide applications of the copper surface. For example, we may take the advantage of the superhydrophobic surface to repel water droplets on such a CuO surface tilted one degree (see movie 1 in the Supporting Information). When heating one end of the sample on an alcohol burner for about 2 s, the temperature in the sample would nonuniformly distributed, the closer to the end, the higher the temperature was. Because the desorption of the low-surface-energy layer depends on the temperature, the temperature gradient leads to the desorption gradient and then the hydrophobicity gradient. Thus, when a droplet drops on the superhydrophobic end of the tilted sample, it slips away because of the high hydrophobicity, while the droplet will be stuck at the less hydrophobic end (see movie 2 in the Supporting Information). For industrial application, we synthesize a large area superhydrophobic panel with such CuO surface coated with the low surface monolayer. By using fire, we may form many circular wettability gradient regions with superhydrophilic cores, as illustrated by Figure 7a. If there is a dewdrop standing on the superdydrophobic region, a little vibration caused by wind will bring it to one of superhydrophilic cores, as demonstrated by droplet one in Figure 7b. If a dewdrop or raindrop directly drops on the gradient region, the difference in the receding angle stepped

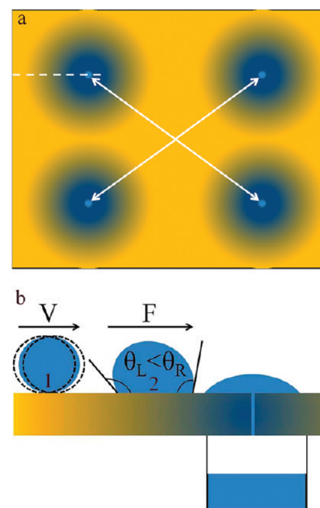

Figure 7. Illustration of the suggested device. (a) The plan view of the device. The circular regions denote the baked superhydrophobic surface of copper. There is a wettability gradient in each region, from superhydrophobicity to superhydrophilicity. Color denotes the degree of wettability. Yellow, superhydrophobicity; blue, superhydrophilicity. The sea blue core denotes the drilled narrow channel. (b) The schematics of the state when dewdrops or raindrops fall on the dash line in a, where droplet 1 who falls on the superhydrophobic surface. It will continue to slip until it is stuck and absorbed at the superhydrophilic region. Droplet 2 falls on the wettability gradient region, in which θ_L and θ_R denote the receding CAs on both sides. The arrow shows the direction of unbalanced Young's force.

from the hydrophobicity gradient, there will be an unbalanced Young's force acting on the droplet and the droplet will be vectored in the direction of decreasing CA, no matter under nonsticking Cassie state or sticking Wenzel state.[43] Finally, the droplets will spontaneously gather at the central and flow into the container through the narrow channel under capillary effect. This device should be very useful to collect dewdrop and raindrop without energy in arid areas.

■ CONCLUDING REMARKS

Appropriate surface roughness and low surface energy are indispensable for superhydrophobicity, whereas the same surface roughness with high surface energy leads to surerhydrophilicity. To achieve the wettability cycling between surperhydrophobicity and superhydrophilicity, the prerequisite is to have appropriate surface roughness. In the present work, chemical etching and electrodeposition were carried out to gain the appropriate surface roughness on copper substrate, which possesses a hierarchical structure combining micro- and/or nanogaps/pores. Due to oxidation, a CuO layer was naturally formed on the hierarchical structure surface at room temperature in air. This hierarchical structure is strong enough to suffer the following treatment for changing the surface chemistry. A HDFT monolayer was self-assembled on the hierarchical structure surface after it was immersed in 1 mM HDFT-ethanol solution for 30 min. This monolayer could be removed by annealing at 200 °C for 10 min, which turns the surface chemical composition back to CuO. By repeating the process of adsorbing/

desorbing of the monolayer, we cycle the surface chemical composition between HDFT and CuO, and then completely change the wettability behavior of the copper surface. This strategy is rapid, only 40 min a cycle, and convenient. Although only Cu surface was studied in this experiment, this strategy could also be extended to other metallic hierarchical structured surfaces[44−46] as long as these materials have the similar properties as Cu. The cycling process could be much faster with other materials if the absorbing and desorbing processes take much shorter time.

■ ASSOCIATED CONTENT

Supporting Information

Movie files (WMV). This material is available free of charge via the Internet at http://pubs.acs.org.

■ AUTHOR INFORMATION

Corresponding Author

*E-mail: mezhangt@ust.hk. Tel: (852) 2358-7192. Fax: (852) 2358-1543.

■ REFERENCES

(1) Acatay, K.; Simsek, E.; Ow-Yang, C.; Menceloglu, Y. Z. *Angew. Chem., Int. Ed.* **2004**, *43*, 5210.
(2) Aristoff, J. M.; Bush, J. W. M. *J. Fluid Mech.* **2009**, *619*, 45.
(3) Bush, J. W. M.; Hu, D. L. *Annu. Rev. Fluid Mech.* **2006**, *38*, 339.
(4) Duez, C.; Ybert, C.; Clanet, C.; Bocquet, L. *Nat. Phys.* **2007**, *3*, 180.
(5) Azzaroni, O.; Brown, A. A.; Huck, W. T. S. *Adv. Mater.* **2007**, *19*, 151.
(6) Bico, J.; Thiele, U.; Quere, D. *Colloids Surf., A* **2002**, *206*, 41.
(7) Caputo, G.; Cortese, B.; Nobile, C.; Salerno, M.; Cingolani, R.; Gigli, G.; Cozzoli, P. D.; Athanassiou, A. *Adv. Funct. Mater.* **2009**, *19*, 1149.
(8) Caputo, G.; Nobile, C.; Kipp, T.; Blasi, L.; Grillo, V.; Carlino, E.; Manna, L.; Cingolani, R.; Cozzoli, P. D.; Athanassiou, A. *J. Phys. Chem. C* **2008**, *112*, 701.
(9) Caputo, G.; Cingolani, R.; Cozzoli, P. D.; Athanassiou, A. *Phys. Chem. Chem. Phys.* **2009**, *11*, 3692.
(10) Feng, X. J.; Jiang, L. *Adv. Mater.* **2006**, *18*, 3063.
(11) Feng, X. J.; Zhai, J.; Jiang, L. *Angew. Chem., Int. Ed.* **2005**, *44*, 5115.
(12) Gu, S. Y.; Wang, Z. M.; Li, J. B.; Ren, J. *Macromol. Mater. Eng.* **2010**, *295*, 32.
(13) Heikenfeld, J.; Dhindsa, M. *J. Adhes. Sci. Technol.* **2008**, *22*, 319.
(14) Lafuma, A.; Quere, D. *Nat. Mater.* **2003**, *2*, 457.
(15) Lahann, J.; Mitragotri, S.; Tran, T. N.; Kaido, H.; Sundaram, J.; Choi, I. S.; Hoffer, S.; Somorjai, G. A.; Langer, R. *Science* **2003**, *299*, 371.
(16) Lifton, V. A.; Taylor, J. A.; Vyas, B.; Kolodner, P.; Cirelli, R.; Basavanhally, N.; Papazian, A.; Frahm, R.; Simon, S.; Krupenkin, T. *Appl. Phys. Lett.* 2008, *93*.
(17) Minko, S.; Muller, M.; Motornov, M.; Nitschke, M.; Grundke, K.; Stamm, M. *J. Am. Chem. Soc.* **2003**, *125*, 3896.
(18) Xia, F.; Zhu, Y.; Feng, L.; Jiang, L. *Soft Matter* **2009**, *5*, 275.
(19) Xin, B. W.; Hao, J. C. *Chem. Soc. Rev.* **2010**, *39*, 769.
(20) Liu, K.; Jiang, L. *Nanoscale* **2011**, *3*, 825.
(21) Burton, Z.; Bhushan, B. *Nano Lett.* **2005**, *5*, 1607.
(22) Shibuichi, S.; Onda, T.; Satoh, N.; Tsujii, K. *J. Phys. Chem.* **1996**, *100*, 19512.
(23) Han, Z. J.; Tay, B.; Tan, C. M.; Shakerzadeh, M.; Ostrikov, K. *Acs Nano* **2009**, *3*, 3031.
(24) Lim, H. S.; Kwak, D.; Lee, D. Y.; Lee, S. G.; Cho, K. *J. Am. Chem. Soc.* **2007**, *129*, 4128.
(25) Jiang, W. H.; Wang, G. J.; He, Y. N.; Wang, X. G.; An, Y. L.; Song, Y. L.; Jiang, L. *Chem. Commun.* **2005**, 3550.
(26) Krupenkin, T. N.; Taylor, J. A.; Wang, E. N.; Kolodner, P.; Hodes, M.; Salamon, T. R. *Langmuir* **2007**, *23*, 9128.
(27) Liang, L.; Rieke, P. C.; Fryxell, G. E.; Liu, J.; Engehard, M. H.; Alford, K. L. *J. Phys. Chem. B* **2000**, *104*, 11667.
(28) Shi, F.; Song, Y. Y.; Niu, H.; Xia, X. H.; Wang, Z. Q.; Zhang, X. *Chem. Mater.* **2006**, *18*, 1365.
(29) Miyauchi, M.; Nakajima, A.; Watanabe, T.; Hashimoto, K. *Chem. Mater.* **2002**, *14*, 2812.
(30) Wang, L.; Guo, S. J.; Hu, X. G.; Dong, S. J. *Electrochem. Commun.* **2008**, *10*, 95.
(31) Mumm, F.; van Helvoort, A. T. J.; Sikorski, P. *Acs Nano* **2009**, *3*, 2647.
(32) Gu, C. D.; Zhang, J.; Tu, J. P. *J. Colloid Interface Sci.* **2010**, *352*, 573.
(33) Liu, J. P.; Huang, X. T.; Li, Y. Y.; Li, Z. K.; Chi, Q. B.; Li, G. Y. *Solid State Sci.* **2008**, *10*, 1568.
(34) Pan, Q. M.; Jin, H. Z.; Wang, H. *Nanotechnology* **2007**, *18*, 355605.
(35) Li, Y.; Jia, W. Z.; Song, Y. Y.; Xia, X. H. *Chem. Mater.* **2007**, *19*, 5758.
(36) Shirtcliffe, N. J.; McHale, G.; Newton, M. I.; Perry, C. C. *Langmuir* **2005**, *21*, 937.
(37) Shirtcliffe, N. J.; McHale, G.; Newton, M. I.; Chabrol, G.; Perry, C. C. *Adv. Mater.* **2004**, *16*, 1929.
(38) Shirtcliffe, N. J.; McHale, G.; Newton, M. I.; Zhang, Y. *ACS Appl. Mater. Interfaces* **2009**, *1*, 1316.
(39) Shin, H. C.; Dong, J.; Liu, M. L. *Adv. Mater.* **2003**, *15*, 1610.
(40) Sung, M. M.; Sung, K.; Kim, C. G.; Lee, S. S.; Kim, Y. *J. Phys. Chem. B* **2000**, *104*, 2273.
(41) Keller, H.; Simak, P.; Schrepp, W.; Dembowski, J. *Thin Solid Films* **1994**, *244*, 799.
(42) Ron, H.; Cohen, H.; Matlis, S.; Rappaport, M.; Rubinstein, I. *J. Phys. Chem. B* **1998**, *102*, 9861.
(43) Wu, J.; Ma, R.; Wang, Z.; Yao, S. *Appl. Phys. Lett.* **2011**, *98*, 204104.
(44) Larmour, I. A.; Saunders, G. C.; Bell, S. E. J. *New J. Chem.* **2008**, *32*, 1215.
(45) Gu, C. D.; Xu, X. J.; Tu, J. P. *J. Phys. Chem. C* **2010**, *114*, 13614.
(46) Gu, C.; Tu, J. *Langmuir* **2011**, *27*, 10132.